arXiv:astro-ph/0011229v1 11 Nov 2000

Turbulent Fragmentation and the Initial Conditions for Star Formation

Paolo Padoan
Harvard-Smithsonian Center for Astrophysics, Cambridge, MA 02138, USA

Åke Nordlund
Copenhagen Astronomical Observatory, and Theoretical Astrophysics Center, 2100 Copenhagen, Denmark

Örnólfur Einar Rögnvaldsson
Nordic Institute for Theoretical Physics, 2100 Copenhagen, Denmark

Alyssa Goodman
Harvard-Smithsonian Center for Astrophysics, Cambridge, MA 02138, USA

ABSTRACT

Super–sonic turbulence fragments molecular clouds (MC) into a very complex density field with density contrasts of several orders of magnitude. A fraction of the gas is locked into dense and gravitationally bound cores, which collapse as proto–stars. This process can be studied with numerical simulations of super–sonic self–gravitating turbulence.

In this work, we use numerical simulations of magneto–hydrodynamic (MHD), super–sonic, super–Alfvénic and self–gravitating turbulence to compute the mass distribution of collapsing proto–stellar cores, which are selected as local density maxima. We find that the mass distribution of collapsing cores is consistent with the stellar initial mass function (IMF), suggesting that super–sonic turbulence may be responsible for the generation of the IMF.

To support this conclusion we also show that the physical properties of the numerically selected cores are in agreement with the properties of observed NH_3 cores and that their magnetic field strength is consistent with Zeeman splitting measurements.

In turbulent MCs, star formation occurs via the gravitational collapse of super–critical cores, formed by the turbulent flow, sub–critical cores being irrelevant for the process of star formation.

Subject headings: turbulence – ISM: kinematics and dynamics; radio astronomy: interstellar: lines

1. Introduction

Despite early observational evidence of the highly super–sonic nature of molecular cloud (MC) turbulence (Zuckerman & Palmer 1974), there have been attempts to simplify the problem of star formation by: i) assuming that super–sonic turbulence behaves like sub–sonic laboratory turbulence; or by ii) focusing on the process of the formation of one single star, neglecting its larger scale environment. The first type of simplification has allowed theoreticians to consider super–sonic turbulence as a source of internal pressure, as suggested by Chandrasekhar (1958) for sub–sonic turbulence (e.g. Bonazzola et al. 1987, 1992). This simplification puts aside the most important characteristic of super–sonic turbulence, that is, the generation of a very fragmented density field by a complex system of turbulent shocks. The second type of simplification has allowed for the generation of analytical and numerical models for the collapse of proto–stars, based on quasi statically evolving proto–stellar cores (e.g. Shu, Adams & Lizano 1987), which are hard to reconcile with the turbulent medium from which they are formed. A complementary way to model the dynamics of MCs avoiding the problem of super–sonic turbulence has been the assumption that the observed line width of molecular transitions is not due to turbulence, but to Alfvén waves, that is, oscillations of a rather strong magnetic field (Arons & Max 1975; Zweibel & Josafatsson 1983; Elmegreen 1985; Falgarone & Puget 1986). However, even in this scenario, random motions and super–sonic shocks are generated by super–sonic compressions along magnetic field lines, and so the process of turbulent fragmentation is unavoidable, irrespective of the magnetic field strength.

Recent numerical studies of super–sonic magneto–hydrodynamic (MHD) turbulence have shed new light on the physics of turbulence. The most important results are: i) Super–sonic turbulence decays in approximately one dynamical time, independent of the magnetic field strength (Padoan & Nordlund 1997, 1999; MacLow et al. 1998; Stone, Ostriker & Gammie 1998; MacLow 1999); ii) The probability distribution function of gas density in isothermal turbulence is well approximated by a Log–Normal distribution, whose standard deviation is a function of the rms Mach number of the flow (Vazquez–Semadeni 1994; Padoan 1995; Padoan, Jones & Nordlund 1997; Scalo et al. 1998; Nordlund & Padoan 1999; Ostriker, Gammie & Stone 1999); iii) Super–sonic isothermal turbulence generates a complex system of shocks that fragment the gas very efficiently into high density sheets, filaments, and cores; iv) Super–Alfvénic turbulence provides a good description of the dynamics of MCs, and an explanation for the origin of dense cores with magnetic field strength consistent with Zeeman splitting measurements. (Padoan & Nordlund 1997, 1999).

We call "turbulent fragmentation" the process leading to the generation of high density structures (and low density "voids") by turbulent shocks. In previous works we investigated the possibility that MCs are fragmented primarily by random super–sonic motions, assuming that self–gravity is important only in the densest regions, so we used numerical simulations of turbulent flows where the effects of self–gravity were intentionally disregarded (Padoan, Jones & Nordlund 1997; Padoan et al. 1998, 1999; Padoan & Nordlund 1997, 1999; Padoan, Zweibel & Nordlund 2000; Padoan et al. 2000). We found that many observational properties of MCs are indeed consistent with the properties of turbulent flows, which supports the suggestion that gravity is important only in the densest regions formed by turbulent shocks.

In this work we include the description of self–gravity, in simulations of three dimensional super–sonic MHD turbulent flows (§ 2). Self–gravity is here required because we are interested in selecting gravitationally bound (collapsing) protostellar cores, formed by the process of turbulent fragmentation. The mass distribution of proto–stellar cores, selected numerically as local maxima in the gas density, is computed in § 3. The value of this result is then confirmed by the comparison between the numerically selected cores and the observed NH_3 cores, in § 4. The simulation also allows us to predict core properties, which are difficult to measure observationally and are therefore not well known, such as the magnetic field strength (§ 5). In § 6 we discuss the results of this work, and in § 7 we list our main conclusions.

2. The Numerical Simulations

2.1. The Equations

We solve the compressible MHD equations:

$$\frac{\partial \ln \rho}{\partial t} + \mathbf{v} \cdot \nabla \ln \rho = -\nabla \cdot \mathbf{v}, \qquad (1)$$

$$\frac{\partial \mathbf{v}}{\partial t} + \mathbf{v}\cdot\nabla\mathbf{v} = -\frac{P}{\rho}\nabla \ln P + \frac{1}{\rho}\mathbf{j}\times\mathbf{B} - \nabla\Phi + \mathbf{f}, \quad (2)$$

$$\frac{\partial e}{\partial t} + \mathbf{v}\cdot\nabla e = -\frac{P}{\rho}\nabla\cdot\mathbf{v} + Q_{\rm dissipation} + Q_{\rm radiation}, \quad (3)$$

$$\frac{\partial \mathbf{B}}{\partial t} = \nabla\times\mathbf{v}\times\mathbf{B}, \quad (4)$$

$$\mathbf{j} = \nabla\times\mathbf{B}, \quad (5)$$

$$\nabla^2\Phi = C\rho \quad (6)$$

plus numerical diffusion terms, and with periodic boundary conditions. $\mathbf{v}$ is the velocity, $\mathbf{B}$ the magnetic field, Φ the gravitational potential, $\mathbf{f}$ an external random force, e the internal energy, $P = \rho T$ is the pressure at $T \approx$ const. The isothermal approximation (see discussion in Padoan, Zweibel & Nordlund 2000) makes the energy equation (3) redundant, and so the $Q_{\rm dissipation}$ and $Q_{\rm radiation}$ are not defined here. The constant C is given by:

$$C = \frac{4\pi G l_0^2 \rho_0}{v_0^2}, \quad (7)$$

where the velocity is measured in units of v_0, length in units of l_0, time in units of l_0/v_0, and density in units of ρ_0. If the velocity is measured in units of the sound speed c_s, and the computational box size is $L_0 = N l_0$, where N is the number of computational cells along one dimension of the numerical mesh, the constant C can be expressed as:

$$C = \frac{1}{N^2}\left(\frac{v_{ff}^2}{c_s^2}\right), \quad (8)$$

where v_{ff} is the free–fall time.

2.2. The Model

For the purpose of this paper we have run a numerical simulation of super–sonic, super–Alfvénic and self–gravitating MHD turbulence, by solving numerically the equations given above. As in our previous works, the initial density and magnetic fields are uniform; the initial velocity is random, generated in Fourier space with power only on the large scale. We also apply an external random force, to drive the turbulence at a roughly constant rms Mach number of the flow. This force is generated in Fourier space, with power only on small wave numbers ($1 < k < 2$), as the initial velocity.

We let the flow evolve for one dynamical time. In our previous simulations without self–gravity, we usually let the flow evolve and relax for many dynamical times, since all density structures are transient. With self–gravity this is not possible because the flow does not statistically relax, and continues to generate an increasing number of collapsing cores, and to accrete mass around them. Since our numerical resolution (128^3 numerical mesh) allows only the description of the initial phase of the collapse of single cores (§ 2.3), results are progressively inaccurate at later times, when the numerical resolution cannot cope with the exceedingly high density. We therefore interrupt the simulation at a time when most cores are just recently formed and start to collapse, which is about one dynamical time of the large scale, $t_{dyn} = L_0/\sigma_v$, where L_0 is the linear size of the computational box, and σ_v is the rms flow velocity.

Periodic boundary conditions and large scale external forcing are justified by the fact that we simulate a region of turbulent flow inside a larger turbulent molecular cloud. The rms Mach number of the flow is $\mathcal{M}_s \approx 10$, which corresponds to a linear size $L_0 \approx 5$ pc, and an average gas density $< n > \approx 900$ cm^{-3}, using empirical Larson type relations (e.g. Larson 1981; Myers 1983; Fuller & Myers 1992). The average magnetic field in this model is rather weak, as justified by our previous work (Padoan & Nordlund 1997, 1999), and such that the average magnetic energy is of the order of the average thermal energy. Assuming a kinetic temperature $T = 10$ K, the rms flow velocity is $\sigma_v \approx 2.5$ km/s, and the average magnetic field strength is $\langle B\rangle \approx 4.5$ μG. Despite this low value of $\langle B\rangle$, strongly magnetized cores are formed by the process of turbulent fragmentation (with field strength sometimes in excess of 100 μG), due to local compressions in the turbulent flow.

2.3. Proto–stellar Cores in Numerical Simulations of Super–Sonic Turbulence

Star forming cores in MCs have typical gas density of about 10^4 cm^{-3}, and are part of larger clouds with density of the order of 10^3 cm^{-3}. Although MCs have internal structure that spans a continuous range of gas density, these values are representative of clouds and

cores on the scale probed by ^{13}CO and NH_3 transitions respectively. The initial density of individual proto–stellar cores (approximately 10^5 cm^{-3}) is close to the maximum density achieved by a finite difference MHD code on a 128^3 numerical mesh; when a scale of 5–10 pc and an average density of approximately 10^3 cm^{-3} are simulated. In such a simulation, with an rms Mach number $\mathcal{M}_s \approx 10$, a density contrast of about 5 orders of magnitude is typically achieved from a minimum density of 1 cm^{-3} to a maximum density of 10^5 cm^{-3}. Higher densities, characteristic of collapsing proto-stellar cores, cannot be achieved with such a numerical tool. In a few years numerical simulations of the same sort, in a larger numerical mesh with size of the order of 1000^3, will become generally available and will allow the numerical description of the initial phase of the collapse of proto–stellar cores. The future application of smooth particle hydrodynamic (SPH) codes to the study of super–sonic turbulence with strong radiative cooling (Klessen, Heitsch & Mac Low 2000), or the future development of MHD codes on an adaptive mesh (Truelove et al. 1998) are also promising. Meanwhile, it is possible to investigate the role of self–gravitating turbulence in the formation of proto–stellar cores, even if only the initial conditions for the gravitational collapse of each core can be described numerically. The formation of collapsing cores in numerical simulations of super–sonic turbulence, and their rate of disruption by the turbulent flow, has been previously discussed by Klessen, Heitsch & Mac Low (2000), and Heitsch, Mac Low & Klessen (2000). These works focus on the issue of turbulent and magnetic support against local gravitational collapse. They conclude that local gravitational collapse cannot be avoided unless the turbulence is driven on scales smaller than the local Jeans length in the densest regions, or the magnetic field provides magnetostatic support.

3. The Mass Distribution of Collapsing Cores

In order to select collapsing cores from the numerical simulations, we have defined as cores density fluctuations with an amplitude of at least 2.5%,

$$\frac{\rho_{max} - \rho_{iso}}{\rho_{iso}} \geq 0.025 \qquad (9)$$

where ρ_{max} is the density value at the local density maximum that defines the fluctuation, and ρ_{iso} is the density value of the density isosurface that delimits the mass assigned to the fluctuation. The isosurface is determined as the smallest density such that the whole region inside the isosurface contains only one density maximum that exceeds the isosurface value by 2.5%.

Density fluctuations of a 2.5% amplitude grow to only a 50% amplitude while the collapsing background has increased its density of about 3 orders of magnitude (Tohline 1980). Density fluctuations of smaller amplitude are unlikely to collapse away from the background before they (or the background) become rotationally supported. However, this choice of the 2.5% amplitude threshold is somewhat arbitrary, as discussed below (see § 6). According to the definition of core given above, we do not select cores that are fragmented into smaller ones. If at least two smaller cores are found inside a larger one, the latter is excluded from the sample. Moreover, only cores with gravitational energy in excess of the sum of thermal and magnetic energies are included in the sample because we are interested only in collapsing proto–stellar cores, that is, in super–critical ones. Sub–critical cores are transient density enhancement, which will re-expand or be destroyed by the turbulent flow, or will later accrete more mass in a dynamical time from the random turbulent flow to become super–critical and collapse. There is only a very small chance that sub–critical cores, formed by a turbulent flow, are found in equilibrium and are given the opportunity to maintain such equilibrium, for as long as the ambipolar drift time (cf. Nakano 1998). Therefore, although sub–critical cores can exist as transient structures, they are almost irrelevant to the process of star formation, contrary to the picture once proposed in the literature (Shu, Adams & Lizano 1987).

The mass distribution of collapsing cores, selected from the MHD simulations (MHD cores), is plotted in Figure 1 (left panel), as the number of cores per logarithmic mass interval. Cores above 2 $M_\odot$ are selected by scaling the computational box to a physical size of 15 pc. Cores smaller than 2 $M_\odot$ are selected after rescaling to a physical size of 5 pc. In order to match the two mass distributions, the total number of cores from the small scale has been multiplied by a factor equal to the ratio of the total mass contained in the two models. Since we scale the physical values of the average gas density in the computational box according to a Larson type relation, $n \propto L^{-1}$, the 5 pc model has an average density 3 times larger than the 15 pc model, and thus a total mass 9 times smaller. The number of cores selected from the 5 pc

model has therefore been multiplied by a factor of 9. Each mass distribution extends above and below 2 $M_\odot$, and match almost exactly in the mass range where they overlap. In order to plot them together, we have used only the mass range above 2 $M_\odot$ for the 15 pc model and the mass range below 2 $M_\odot$ for the 5 pc model.

The distribution in Figure 1 is a power law between 2 and 200 $M_\odot$, with a slope, $\Gamma = 1.34$, consistent with the Salpeter stellar initial mass function (IMF), $\Gamma = 1.35$. At about 2 $M_\odot$ the mass distribution flattens, and turns around at about 0.5 $M_\odot$ (in these logarithmic units). The scale–free behavior at large and intermediate masses is due to the process of turbulent fragmentation. The initial flattening at about 2 $M_\odot$ is caused by the magnetic pressure: for increasingly smaller masses, an increasing number of small density enhancements assembled by turbulence are found to be sub–critical (magnetic plus thermal energies in excess of the gravitational energy), and are therefore excluded from the sample because they are not collapsing. The cutoff at the smallest masses is mainly due to the thermal pressure, because most of the smallest cores are smaller than their own Jeans mass and are therefore excluded from the sample of collapsing cores.

In the plot in Figure 1 (left panel) there is no core below 0.2 $M_\odot$. This particular value is set by the numerical resolution of the simulation that does not allow one to discern anything smaller. The actual cutoff, and also the mass of the turn–around of the distribution, should be somewhat smaller. Moreover, it is very likely that even individual proto–stellar cores fragment at least into a binary system. If the mass distribution of each member of a binary system is plotted, instead of the mass distribution of proto–stellar cores, the low mass end of the distribution is much more populated. As an example, we have computed the mass distribution of single components of the binary systems, assuming that each core fragments into two components, whose mass ratio is a uniformly distributed random variable with values between 0 and 1. The result is plotted on the right panel of Figure 1. The mass distribution of single components has its maximum value at approximately 0.3 $M_\odot$, it is almost symmetric around the maximum, and it extends down to sub–stellar masses with a probability comparable to the one of the most massive stars. Expressed in linear mass units (dotted line), the mass distribution is almost flat below the maximum, which is found at approximately 0.2 $M_\odot$.

Finally, the whole distribution should be shifted somewhat towards smaller masses, if it is to be compared with the stellar IMF (for example Luhman et al. 2000) since proto–stellar collapse is always accompanied by mass loss.

4. Numerical Cores and Observed NH_3 Cores

In the previous section we have found that the mass distribution of collapsing cores in the MHD simulation ('MHD cores') is consistent with the stellar IMF. In order to confirm the validity of this result, it is useful to compare the physical properties of the MHD cores, with the properties of cores selected observationally via molecular line transitions. We use the NH_3 core sample from Jijina, Myers & Adams (1999), which is a literature compilation of 264 NH_3 cores. For the purpose of this work, we use 149 cores not associated with stellar clusters, as defined in Jijina, Myers & Adams' sample, because they offer a more appropriate description of the initial conditions of star formation.

Figures 2 and 3 show the probability distribution of the radius, non–thermal line width, velocity gradient (rotation), and gas density of both NH_3 and MHD cores (notice that all the histograms are in log units). Numerical and observed cores are very similar in size, amount of turbulence, rotation, and density. NH_3 cores have slightly larger line width, which could be due to velocity superposition along the line–of–sight of physically unrelated gas. Average values and variances of each histogram are listed in Table 1. Slightly differences between the properties of MHD and NH_3 cores are expected, because the properties of the MHD cores are here obtained directly from the three dimensional numerical data–cubes of density and velocity field. We have not tried to reproduce exactly the observational procedure by solving the radiative transfer through the data–cube. This more detailed comparison with the observations, via the computation of synthetic spectral maps, has been the subject of other works (Padoan et al. 1998, 1999, 2000).

In order to further compare the two core samples, we consider the "Type 2" correlation between size and line width (single–tracer multiple–cloud –Goodman et al. 1998), which we plot in Figure 4. The NH_3 cores without a stellar cluster association are represented by open squares, and the MHD cores by asterisks. A least square fit is also shown for both samples. The

line width versus size relations are remarkably similar; the slope is (0.56±0.22) for the NH_3 cores, and (0.57± 0.15) for the MHD cores (Table 1).

5. Magnetic Fields in Proto–Stellar Cores

The magnetic field strength, B, in proto–stellar cores is usually unknown, because it is very difficult to measure observationally. In order to compare B in MHD cores with the observations, we need to refer to the few available detections and upper limits of B, which are based on OH or CN Zeeman splitting measurements, although such measurements apply to a variety of scales, and not just to proto–stellar cores. In Figure 5 we have plotted B versus the estimated H_2 column density, using a sample of Zeeman splitting measurements from Bourke et al. (2000), which contains the previous sample by Crutcher (1999), a number of original detections and upper limits and the recent detections by Crutcher & Troland (2000) in L1544 and by Sarma et al. (2000) in NGC6334. Asterisks represent detections and triangles upper limits (19 detections and 31 upper limits). From the point of view of this work (see below), a conservative choice is to assume that the magnetic field strength is in all cases very close to the estimated upper limits. The dashed line in Figure 5 is a least square fit to the observations, where upper limits have been treated as if they were detections.

The numerical cores, represented by squares in Figure 5, follow almost exactly the same B–N_{col} relation as the observations (the solid line is their least square fit). We have also plotted in the same figure the line that marks the equality between magnetic and gravitational energies, $\mathcal{M} = \mathcal{W}$. All magnetic field detections but one are below that line, which means that all regions observed have gravitational energy in excess of the magnetic energy, and only 3 of the 31 upper limits and 1 of the 19 detections are above the line. Of the 80 numerical cores, only 3 are above the line. All numerical cores, including those three, are super–critical (gravitational energy in excess of the magnetic energy) and have been selected as such. They can be occasionally found above the line because they are elongated along the direction of the magnetic field (aspect ratio 2–3), which decreases their critical mass, relative to that of a spherical core with the same B (McKee et al. 1993). Notice that several MHD cores with relatively large values of B are found, even in excess of 100 μG, although the average B in the simulation is only 4.5 μG, making the large scale turbulence super–Alfvénic (Padoan & Nordlund 1999).

6. Discussion

In this work we have found that the mass distribution of collapsing cores is practically indistinguishable from the stellar IMF. This suggests that turbulent fragmentation is an essential ingredient in the generation of the stellar IMF. The computation of the mass distribution of cores relies on the selection of local maxima of the gas density in numerical simulations of super–sonic turbulence. This method contains some uncertainties, the most significant being the assumption that any single core, corresponding to a density fluctuation beyond a threshold amplitude, collapses as a single proto–star or as a binary system, if it is not initially fragmented into smaller fluctuations with amplitude larger than the same threshold. The particular value of the threshold of 2.5% is justified by the fact that fluctuations of smaller amplitude would hardly grow before they become rotationally supported. However, the true value could be anything between 1% and 4%, and may also have spatial variations. A smaller amplitude threshold produces a steeper mass distribution than a larger threshold, because it selects a larger number of smaller cores. The slope, which we found to be 1.34 for a 2.5% threshold, could therefore be anything between 1.2 and 1.5.

Recent observational data seem to confirm the present result, that is, turbulent fragmentation generates a mass distribution of proto–stellar cores very similar to the stellar IMF. Dust continuum observations (Motte, Andre & Neri 1998) and high density molecular tracers (Ohnishi et al. 2000), have shown that dense cores in MCs have a mass distribution consistent with the stellar IMF.

We have considered only super–critical cores, because they collapse and form stars. This is in sharp contrast with the usual description of low mass star formation as the result of the quasi–static evolution of sub–critical cores. The primary reason we do not consider sub–critical cores is that they are transient structures in a super–sonic turbulent flow. Sub–critical cores disperse, re–expand, or accrete more mass from the turbulent flow and become super–critical and collapse. The last possibility –accreting more mass– is in fact the usual mode of formation of super–critical cores, and it is a dynamical process, controlled by the turbulent flow. It is highly unlikely

that a sub–critical core is formed in equilibrium at all, and even more unlikely that it is left undisturbed for as long as the ambipolar drift time–scale, as assumed in many low mass star formation theories.

We have shown that a super–sonic turbulent flow generates super–critical cores of very small mass, in the same proportion as required by the stellar IMF. There is, therefore, no "need" to form low mass stars from sub–critical cores. This new point of view on star formation suggests that star formation is a fast process, as also proposed by Ballesteros–Paredes, Hartmann & Vázquez–Semadeni (1999), Elmegreen (2000), and Hartmann (2000). Notice, however, that fast does not mean efficient. As an example, the mass distribution of collapsing cores presented in Figure 1 contains only ≈2% of the total mass in the simulation, which means that in a typical MC, after one dynamical time of the large scale, only a few percent of the total mass is locked into collapsing cores. Star formation is therefore inefficient on the scale of MCs because it occurs only on a small fraction of the total mass. This is ultimately the most important feature of super–sonic turbulence: the density field fragments in a very intermittent way, such that a significant mass fraction is found at densities irrelevant for the process of star formation, or inside very small dense cores that are sub–critical and therefore transient (they do not form stars).

The fast evolution of cores is also suggested by an extremely small fraction of starless cores in the sample of NH_3 cores by Jijina, Myers & Adams (1999), and by the observed chemical abundances in dense cores (Bergin et al. 1997). Finally, we have shown that all Zeeman splitting measurements are consistent with cores being super–critical (Figure 5).

7. Conclusions

We have computed physical properties of collapsing cores, in a simulation of super–sonic, super–Alfvénic, self–gravitating MHD turbulence. The main results are: i) The mass distribution of collapsing MHD cores is consistent with the stellar IMF; ii) The size, density, line width and velocity gradient of MHD and NH_3 cores are very similar; iii) MHD cores and observed NH_3 cores show the same correlation between line width and size; iv) Proto–stellar cores with significant magnetic field strength, even in excess of 100 μG, are formed in a flow with a low average field strength, $\langle B \rangle \approx 4.5$ μG; v) MHD cores show the same relation between magnetic field strength and column density as estimated with Zeeman splitting measurements.

The general conclusion is that turbulent fragmentation is essential to understand the generation of the stellar IMF. Furthermore, star formation, independent of the stellar mass, occurs via the collapse of super–critical cores formed inside super–sonic turbulent MCs, sub–critical cores being irrelevant for the process of star formation. This point of view conflicts with many years of literature on star formation, but it is very promising. It has become accessible to investigation only in the past few years, because of important advances in the field of numerical fluid–dynamics, due to the increased power of super–computers and three–dimensional visualization software.

This work was supported by NSF grant AST-9721455. Åke Nordlund acknowledges partial support by the Danish National Research Foundation through its establishment of the Theoretical Astrophysics Center.

REFERENCES

Arons, J., Max, C. E. 1975, ApJ, 196, L77

Ballesteros-Paredes, J., Hartmann, L., Vázquez-Semadeni, E. 1999, ApJ, 527, 285

Bergin, E. A., Goldsmith, P. F., Snell, R. L., Langer, W. D. 1997, ApJ, 482, 285

Bonazzola, S., Falgarone, E., Heyvaerts, J., Perault, M., Puget, J. L. 1987, A&A, 172, 293

Bonazzola, S., Perault, M., Puget, J. L., Heyvaerts, J., Falgarone, E., Panis, J. F. 1992, J. Fluid Mech., 245, 1

Bourke, T., Myers, P., Robinson, G., Hyland, H. 2000, in preparation

Chandrasekhar, S. 1958, Proc. Roy. Soc., 246, 301

Crutcher, R. M. 1999, ApJ, 520, 706

Crutcher, R. M., Troland, T. H. 2000, in preparation

Elmegreen, B. G. 1985, ApJ, 299, 196

Elmegreen, B. G. 2000, ApJ, 530, 277

Falgarone, E., Puget, J. L. 1986, A&A, 162, 235

Fuller, G. A., Myers, P. C. 1992, ApJ, 384, 523

Goodman, A. A., Barranco, J. A., Wilner, D. J., Heyer, M. H. 1998, ApJ, 504, 223

Hartmann, L. 2000, in F. Favata, A. A. Kaas, A. Wilson (eds.), Star formation from the small to the large scale, 33rd ESLAB symp., ESA

Jijina, J., Myers, P. C., Adams, F. C. 1999, ApJS, 125, 161

Klessen, R. S., Heitsch, F., Mac Low, M. 2000, ApJ, 535, 887

Larson, R. B. 1981, MNRAS, 194, 809

Luhman, K. L., Rieke, G. H., Young, E. T., Cotera, A. S., Chen, H., Rieke, M. J., Schneider, G., Thompson, R. I. 2000, astro-ph/0004386

Mac Low, M. 1999, ApJ, 524, 169

Mac Low, M., Smith, M. D., Klessen, R. S., Burkert, A. 1998, ApJS, 261, 195

McKee, C., Zweibel, E., Goodman, A., Heiles, C. 1993, in E. H. Levy, J. I. Lunine (eds.), Protostars and Planets III, (University of Arizona Press, 327

Motte, F., Andre, P., Neri, R. 1998, A&A, 336, 150

Myers, P. C. 1983, ApJ, 270, 105

Nakano, T. 1998, ApJ, 494, 587

Nordlund, Å., Padoan, P. 1999, in J. Franco, A. Carramiñana (eds.), Interstellar Turbulence, Cambridge University Press, 218

Ohnishi, T. et al. 2000, preprint

Ostriker, E. C., Gammie, C. F., Stone, J. M. 1999, ApJ, 513, 259

Padoan, P. 1995, MNRAS, 277, 377

Padoan, P., Bally, J., Billawala, Y., Juvela, M., Nordlund, Å. 1999, ApJ, 525, 318

Padoan, P., Jones, B., Nordlund, Å. 1997, ApJ, 474, 730

Padoan, P., Juvela, M., Bally, J., Nordlund, Å. 1998, ApJ, 504, 300

Padoan, P., Nordlund, Å. 1997, astro–ph/9706176

Padoan, P., Nordlund, Å. 1999, ApJ, 526, 279

Padoan, P., Zweibel, E., Nordlund, Å. 2000, ApJ, 540, 332

Padoan, P., Goodman, A., Nordlund, Å., Juvela, M. 2000, ApJ, (submitted)

Sarma, A. P., Troland, T. H., Roberts, D. A., Crutcher, R. M. 2000, ApJ, 533, 271

Scalo, J. M., Vázquez-Semadeni, E., Chappell, D., Passot, T. 1998, ApJ, 504, 835

Shu, F. H., Adams, F. C., Lizano, S. 1987, ARA&A, 25, 23

Stone, J. M., Ostriker, E. C., Gammie, C. F. 1998, ApJ, 508, L99

Tohline, J. E. 1980, ApJ, 239, 417

Truelove, J. K., Klein, R. I., McKee, C. F., Holliman, J. H., Howell, L. H., Greenough, J. A., Woods, D. T. 1998, ApJ, 495, 821

Vázquez-Semadeni, E. 1994, ApJ, 423, 681

Zuckerman, B., Palmer, P. 1974, ARA&A, 12, 279

Zweibel, E. G., Josafatsson, K. 1983, ApJ, 270, 511

This 2-column preprint was prepared with the AAS LaTeX macros v4.0.

TABLE AND FIGURE CAPTIONS:

Table 1: Average values of core property distributions.

Figure 1: Left: Mass distribution of MHD cores. The selection of cores is incomplete at masses $< 0.5 M_{\odot}$ (vertical dotted line), and no core is found below $< 0.2 M_{\odot}$, because of the limited numerical resolution. Right: Mass distribution of single components of the binary systems, assuming that all cores fragment into a binary system, and that the mass ratio of the two components is a uniformly distributed random variable with values between 0 and 1. The dotted line shows the distribution computed in linear mass units.

Figure 2: Left: Probability distribution of core radii. Right: Probability distribution of core line width.

Figure 3: Left: Probability distribution of core velocity gradient. Right: Probability distribution of core density.

Figure 4: Non–thermal line width versus size for numerical cores (asterisks) and observed NH_3 cores (squares).

Figure 5: Magnetic field strength versus H_2 column density. Asterisks represent the Zeeman splitting measurements, and triangles upper limits (19 detections and 31 upper limits). The dashed line is a least square fit to the Zeeman splitting measurements, where upper limits have been treated as if they were detections. The solid line is a least square fit to the MHD cores (squares). The dotted–dashed line marks the equality between magnetic and gravitational energies.

Cores	R [pc]	Δv [km/s]	∇v [km/(s pc)]	n [10^4 cm^{-3}]	Δv–R slope
NH_3	0.11 ± 0.07	0.48 ± 0.33	1.42 ± 1.39	3.3 ± 4.0	0.56 ± 0.22
MHD	0.09 ± 0.06	0.33 ± 0.18	1.84 ± 1.56	3.0 ± 2.2	0.57 ± 0.15

Table 1:

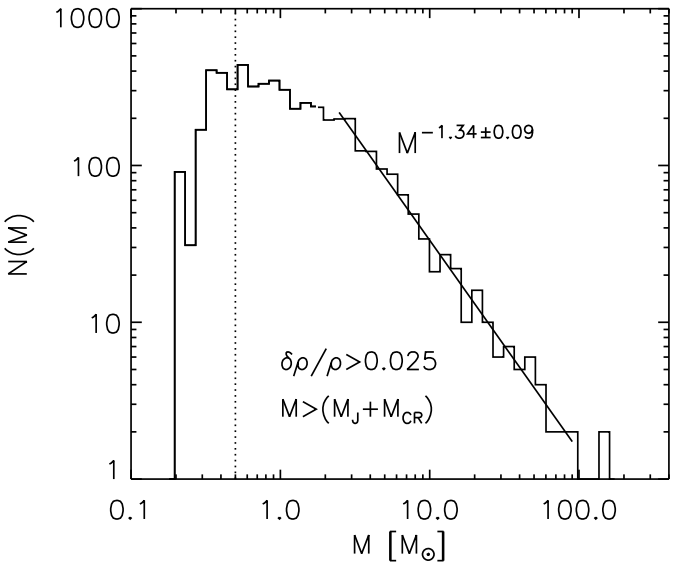
1000
100
10
1
N(M)
0.1
1.0
10.0
100.0
M [M⊙]
M^−1.34±0.09
δρ/ρ>0.025
M>(M_J+M_CR)

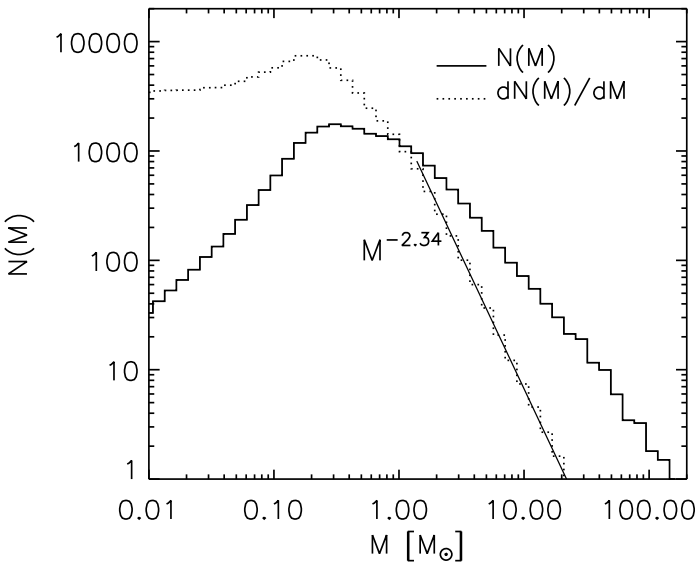
10000
1000
100
10
1
N(M)
0.01
0.10
1.00
10.00
100.00
M [M⊙]
N(M)
dN(M)/dM
M^−2.34

Fig. 1.—

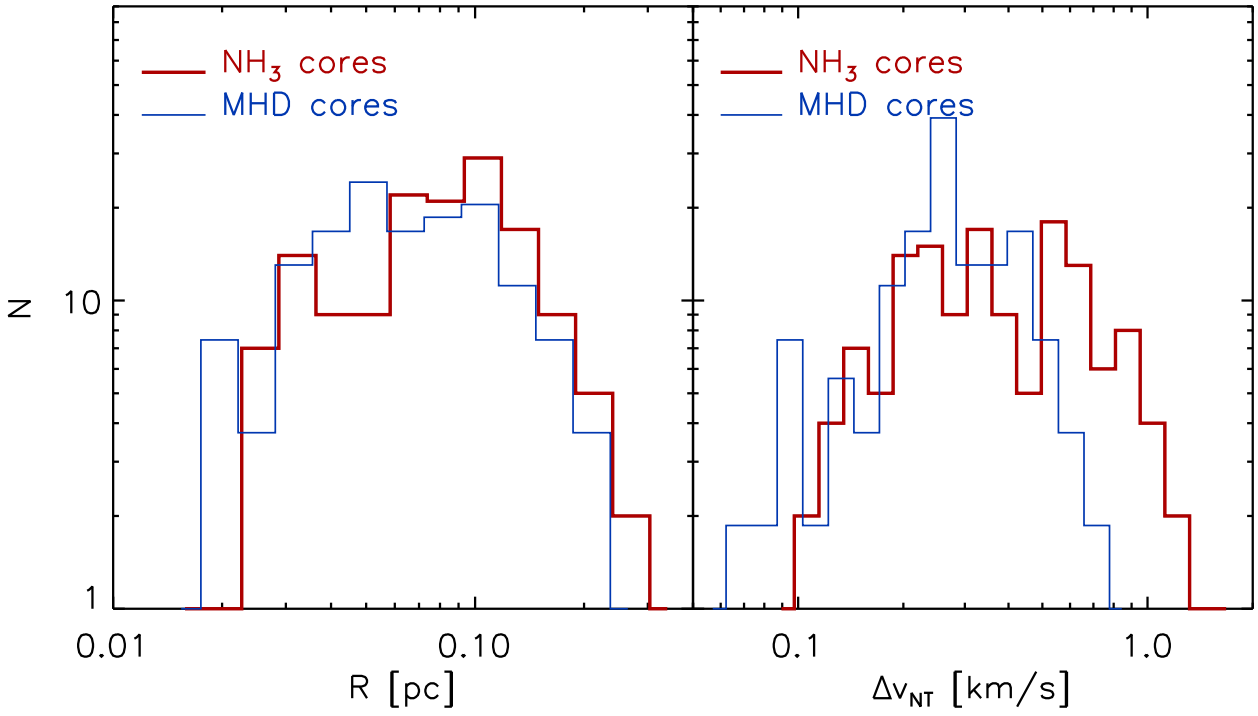
NH3 cores
MHD cores
N
10
1
0.01
0.10
R [pc]
NH3 cores
MHD cores
0.1
1.0
ΔvNT [km/s]

Fig. 2.—

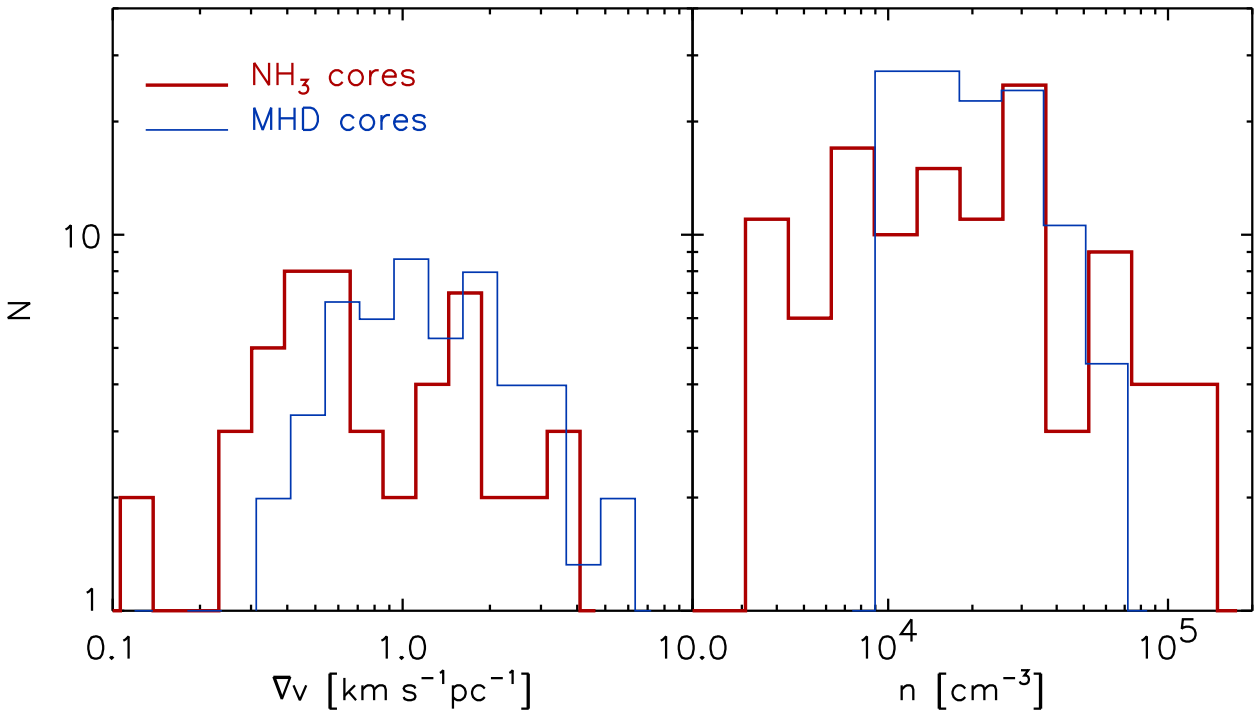

Fig. 3.—

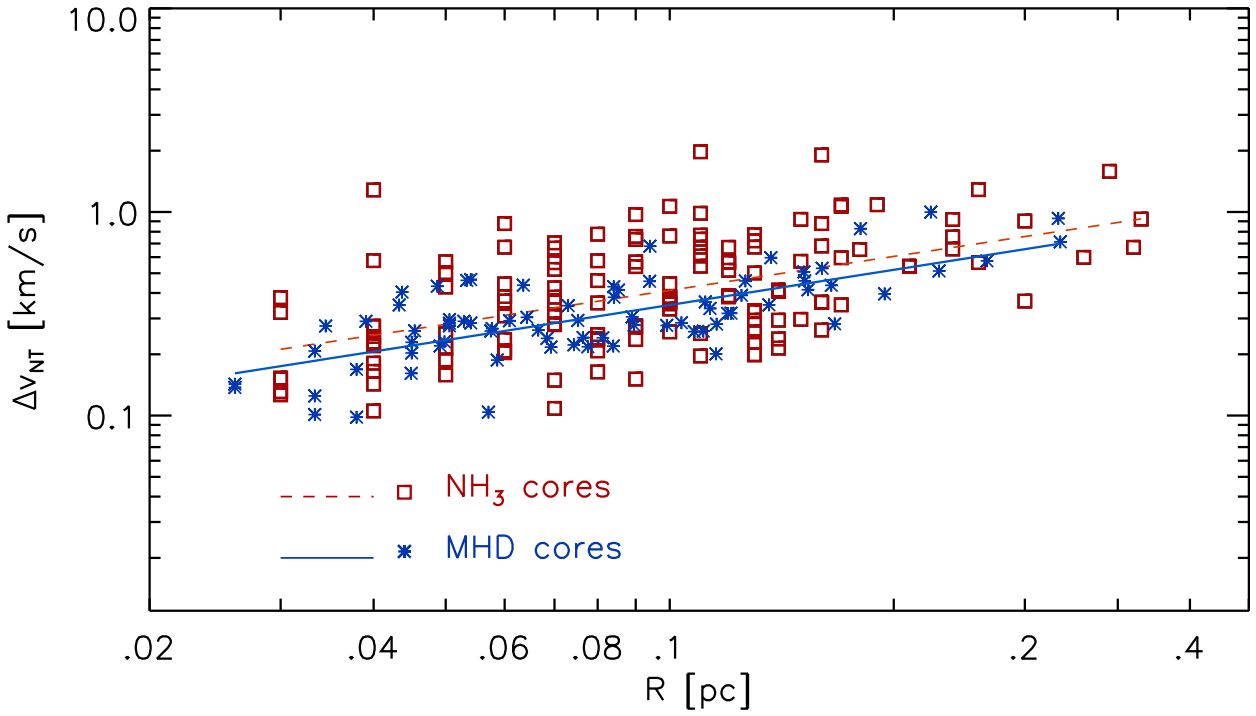

Fig. 4.—

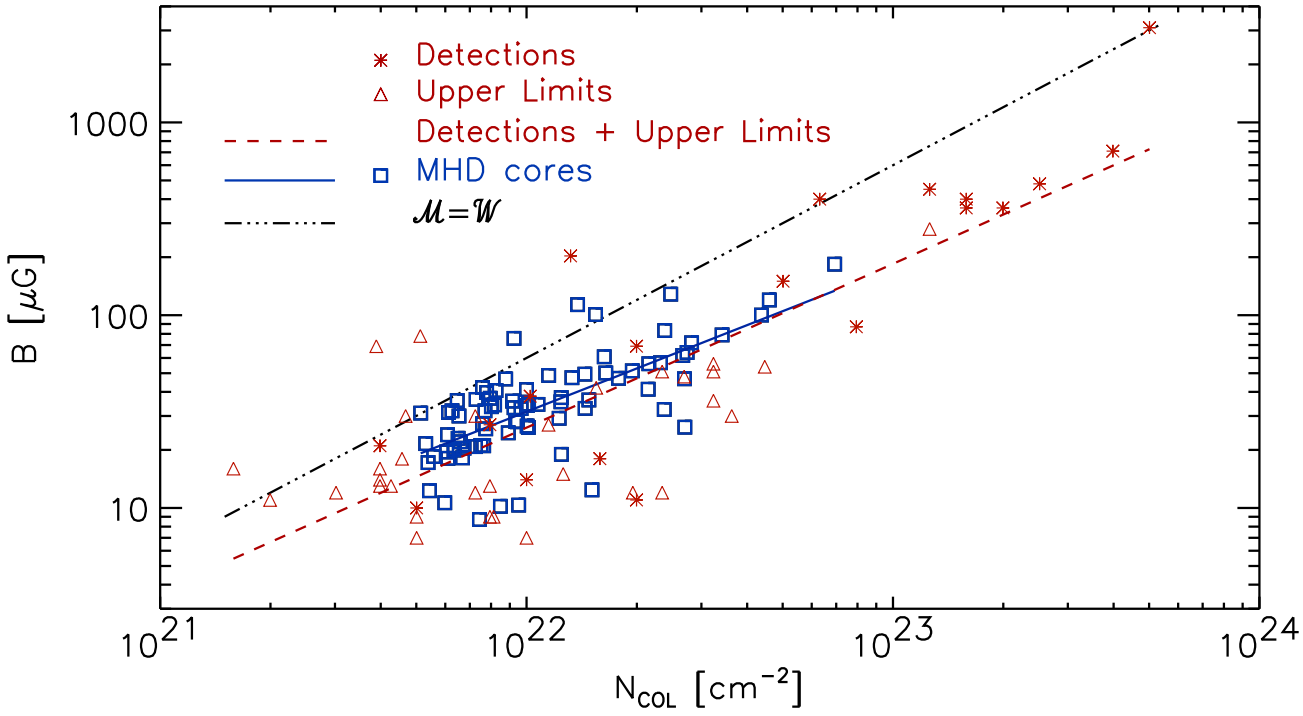
Detections
Upper Limits
Detections + Upper Limits
MHD cores
$\mathcal{M}=\mathcal{W}$
1000
100
10
B [μG]
10^{21}
10^{22}
10^{23}
10^{24}
N_{COL} [cm^{-2}]

Fig. 5.—